

Transition metal oxides as the buffer layer for polymer photovoltaic cells

Vishal Shrotriya, Gang Li, Yan Yao, Chih-Wei Chu, and Yang Yang^{a)}

Department of Materials Science and Engineering, University of California, Los Angeles, Los Angeles, California 90095

(Received 27 May 2005; accepted 28 December 2005; published online 16 February 2006)

Polymer-based photovoltaic cells have been fabricated by inserting a thin, transparent, transition metal oxide layer between the transparent anode (indium tin oxide) and the polymer layer. Two different transition metal oxides, namely vanadium oxide and molybdenum oxide, were used and the device performance was compared. The surface of the oxide films and the interface between the polymer and the oxide was studied with the help of atomic force microscopy. The effect of the thickness of the oxide layer on electrical characteristics of the device was also studied and optimized thickness was achieved to give high power conversion efficiency of 3.3% under simulated AM1.5G illumination of 100 mW/cm². © 2006 American Institute of Physics. [DOI: 10.1063/1.2174093]

Polymer bulk heterojunction (BHJ) photovoltaic (PV) cells have generated a lot of interest for application as a renewable, nonconservative, and truly clean source of energy.^{1–8} Under illumination, the charges are generated in the active layer as a result of photoexcitation, and are subsequently collected at the electrodes. Indium tin oxide (ITO) is used as the transparent hole collecting anode and a low work function metal is used as the electron collecting cathode. It has been demonstrated that using an ITO surface coated with a buffer layer as the anode results in enhanced device performance.⁹ The external quantum efficiency of polymer PV cells is greatly improved when poly(ethylenedioxythiophene) doped with poly(styrenesulfonate) (PEDOT:PSS) is used as a buffer between ITO and the active polymer layer.^{10–12} However, the interface between ITO and PEDOT:PSS is not stable and the chemical reaction between ITO and PEDOT can result in degraded device performance.^{13–15} Several metal oxides have been demonstrated as efficient hole injection materials for organic electroluminescent devices.^{16–18} In this work, we show that transition metal oxides, vanadium oxide (V₂O₅) and molybdenum oxide (MoO₃), can effectively substitute PEDOT:PSS as the buffer layer in the polymer PV cells.

The polymer PV cells in this study consist of a layer of P3HT/PCBM blend thin film sandwiched between ITO and a metal cathode. The energy level diagrams of different materials used in the device fabrication are shown in Fig. 1. For the buffer layer, three different materials were used, namely, PEDOT:PSS, V₂O₅, and MoO₃. A PEDOT:PSS layer of about 25 nm thickness was obtained by spin coating an aqueous solution (Baytron P VP Al 4083) onto ITO coated glass substrates, followed by baking at 120 °C for 1 h. V₂O₅ and MoO₃ layers were thermally evaporated onto ITO substrates under a vacuum of ~10⁻⁶ Torr. To make P3HT/PCBM 1:1 weight-ratio solution, P3HT was first dissolved in 1,2-dichlorobenzene to which PCBM powder was subsequently added. The blend was then stirred for about 12 h at 40 °C in the glove box before spin coating. Finally the cathode, made of 25 nm of Ca and 100 nm of Al, was thermally deposited on top of the active layer in a deposition chamber in the

glove box under a vacuum of ~10⁻⁶ Torr. The device were annealed (post production) at 110 °C for 10 min inside the glove box before electrical characterization. The active area of the device, defined by shadow mask, was 0.105 cm². The *I*-*V* curves were measured by a Keithley 2400 source meter. The photocurrent was measured under illumination from a ThermoOriell 150 W solar simulator with AM1.5G filters, the light intensity of which was measured by a calibrated silicon detector. The atomic force microscopy (AFM) images were obtained using a Digital Instruments multimode scanning probe microscope.

The *I*-*V* characteristics under illumination for the PV devices with various buffer layers are shown in Fig. 2. For the device with UV-ozoned ITO as the anode the power conversion efficiency (PCE) is less than 2.0%. Although the short circuit current density (*I*_{SC}) is high (~7.8 mA/cm²) the open circuit voltage (*V*_{OC}) and FF are comparatively low at 0.49 V and 51%, respectively. Inserting a metal oxide buffer layer between ITO and polymer results in increased *V*_{OC} and FF values for both the oxides used, i.e., V₂O₅ and MoO₃. The *V*_{OC} and FF values are 0.59 V and 59%, respectively, for V₂O₅ (~3 nm), and 0.60 V and 62% for MoO₃ (~5 nm). The *I*_{SC} also increases to 8.83 and 8.94 mA/cm² for V₂O₅ and MoO₃, respectively. As a result, the PCE of devices with metal oxide buffer layers increases to more than 3.0%. The

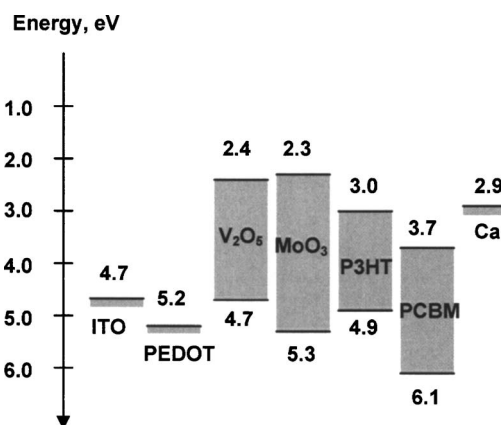


FIG. 1. A schematic showing energy levels of the bottom electrode ITO, various buffer layer materials (PEDOT:PSS, V₂O₅, MoO₃), donor polymer P3HT, acceptor PCBM, and top electrode Ca.

^{a)} Author to whom correspondence should be addressed; electronic mail: yangy@ucla.edu

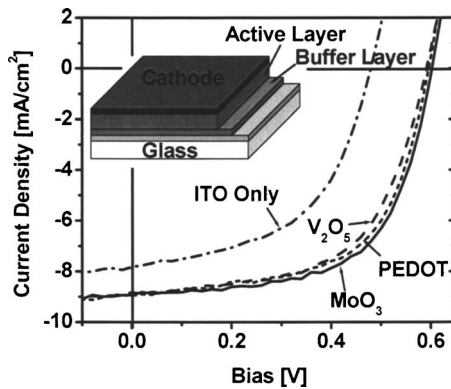


FIG. 2. I - V characteristics of PV devices under illumination for a device with different types of anodes, namely, ITO only, ITO with PEDOT:PSS (25 nm), ITO with V_2O_5 (3 nm), and ITO with MoO_3 (5 nm).

highest PCE of 3.3% is recorded for the devices with MoO_3 buffer layer thickness of ~ 5 nm. Also shown in Fig. 2 is the I - V curve for device with ITO/PEDOT:PSS anode for comparison. The PCE of this device is 3.2%, with $I_{SC} = 8.95$ mA/cm², $V_{OC} = 0.59$, and $FF = 60\%$. These results show that both metal oxides, V_2O_5 and MoO_3 , can substitute PEDOT:PSS as the buffer layer between ITO and the polymer layer with comparable, or as in case of MoO_3 , even better device performance. Interestingly, V_{OC} is the same for all devices with different buffer layers, irrespective of the work function of the buffer material, which were 4.7 eV (V_2O_5), 5.3 eV (MoO_3), and 5.2 eV (PEDOT:PSS). (The work functions of V_2O_5 and MoO_3 were measured in our lab using ultraviolet photoelectron spectroscopy.) This suggests that the V_{OC} of the device is independent of the work function of the anode material. This is very different from the former study by Brabec *et al.*⁵ in which they found a variation of the work function of the anode linearly influences the V_{OC} , with a scaling factor of 0.8. In Ref. 5, the authors suggest that the work function of PEDOT is not pinned to any of the energy levels in the active layer, hence, the variation in V_{OC} . It has been reported earlier^{19,20} that the work function of the cathode metal slightly affects the V_{OC} of the PV cell. One possible explanation for the observed independence of V_{OC} on the buffer layer in our case is the Fermi-level pinning^{21,22} of the metal oxide work function at the highest occupied molecular orbital (HOMO) level of p -type polymer P3HT due to the presence of donor surface states. It is widely believed that the V_{OC} of polymer bulk-heterojunction PV devices depends mainly on the relative energy levels of the donor and acceptor.²³ In our devices, while different buffer layers are used as the bottom contact, the donor and acceptor materials are the same for all devices. Therefore, the V_{OC} being independent of the buffer layer work function is understandable. The summary of various device parameters for all types of devices made in this study is given in Table I. It is important to take into consideration the energy levels of the materials, including the buffer layer, when designing the PV device. The holes, which transport through the P3HT network, will be collected at the anode. As shown in Fig. 1, the HOMO level of P3HT is 4.9 eV. V_2O_5 (HOMO ~ 4.7 eV) and MoO_3 (HOMO ~ 5.3 eV) both form efficient hole injection/collection contact with the active layer. For comparison the HOMO level of PEDOT:PSS is 5.2 eV.

Introducing V_2O_5 or MoO_3 buffer layers will contribute to the series resistance (R_s) of the device and higher thick-

TABLE I. Device operation parameters for devices with different types of anodes fabricated in this study. The numbers in bold represent devices whose I - V characteristics that are plotted in Fig. 2.

Anode	I_{sc} (mA/cm ²)	V_{oc} (V)	FF (%)	PCE (%)
ITO only	7.82	0.49	51.1	1.96
ITO/PEDOT:PSS (25 nm)	8.95	0.59	59.6	3.18
ITO/ V_2O_5 (1 nm)	8.86	0.59	47.5	2.48
ITO/V_2O_5 (3 nm)	8.83	0.59	59.1	3.10
ITO/ V_2O_5 (5 nm)	8.54	0.59	57.2	2.88
ITO/ V_2O_5 (10 nm)	8.16	0.59	57.9	2.79
ITO/ MoO_3 (1 nm)	8.75	0.53	42.3	1.98
ITO/ MoO_3 (3 nm)	8.86	0.59	58.3	3.06
ITO/MoO_3 (5 nm)	8.94	0.60	61.9	3.33
ITO/ MoO_3 (10 nm)	8.73	0.60	59.8	3.13
ITO/ MoO_3 (20 nm)	8.19	0.58	59.9	2.86

ness may result in lower current. An increase in R_s will also lower the FF of the devices.²⁴ On the other hand, a sufficient oxide layer thickness is required to form a uniform contact with the polymer to reduce leakage current. Therefore, it is necessary to optimize the metal oxide layer thickness in order to obtain optimum device performance. The I - V characteristics of devices with different oxide layer thickness are shown in Fig. 3. For V_2O_5 the optimum thickness is 3 nm [from Fig. 3(a)], and for MoO_3 the optimum thickness is 5 nm [Fig. 3(b)]. For both the oxides, when the thickness is about 1 nm or less, the ITO substrate is only partially covered with the oxide forming small islands instead of a uniform film. As a result, the anode/polymer contact has two different interfaces: ITO/polymer and ITO/oxide/polymer. The I - V curves for devices with 1 nm oxide layer can be thought of as two separate curves overlapping each other, each with a different characteristic corresponding to the ITO/polymer and ITO/oxide/polymer contacts. Since the V_{OC} 's for these two curves are different, the overlap of

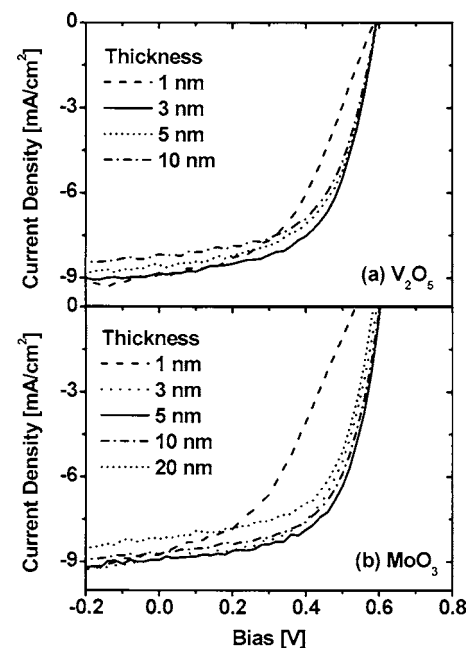


FIG. 3. I - V characteristics under illumination for devices with different thicknesses of (a) V_2O_5 and (b) MoO_3 used as the buffer layer between the ITO and the active layer.

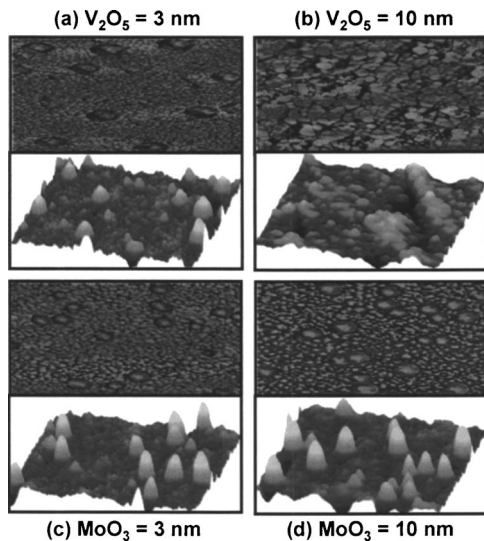


FIG. 4. AFM images of transition metal oxides evaporated on top of the ITO surface: (a) 3 nm V_2O_5 , (b) 10 nm V_2O_5 , (c) 3 nm MoO_3 , and (d) 10 nm MoO_3 . The upper half in each template shows the phase image whereas the lower half shows the height image. All the images were obtained for $1 \mu m \times 1 \mu m$ surface area.

the two competing curves will give the visible concave feature in the resultant I - V curve of the device and as a result a poor FF.

Figure 4 shows the AFM images of $1 \mu m \times 1 \mu m$ ITO surface area, covered with V_2O_5 and MoO_3 , deposited by thermal evaporation. The upper half in each template shows the phase image and the lower half shows the height image for the same scan. After depositing 3 nm of V_2O_5 , small islands of the oxide with a feature size of about 100 nm can be observed on the surface as shown in the bottom half of Fig. 4(a). As a result the surface rms roughness, σ_{RMS} , is ~ 4.7 nm which is about three times the roughness of the ITO surface ($\sigma_{RMS} \sim 1.6$ nm). There are two possibilities for the film below these islands: ITO or metal oxide. The fact that the islands occupy a very small amount of surface area indicates the film below the islands should dominate the performance. The I - V curve of the device with 3 nm metal oxide thus strongly indicates that these islands are formed on top of the oxide film which covers the ITO surface. When the V_2O_5 thickness is 10 nm, the film surface is more uniform as shown in Fig. 4(b) with $\sigma_{RMS} \sim 3.7$ nm. The phase image also shows that the domain size is now bigger. Similar island formation is observed for the MoO_3 films deposited on an ITO surface as shown in Figs. 4(c) and 4(d). The σ_{RMS} is measured to be roughly 6.9 nm for 3 nm of the MoO_3 film which increases to ~ 7.2 nm for 10 nm thickness. Since no island formation was observed for the pristine ITO surface (not shown here), it can be concluded that the islands were made of oxide molecules aggregated together on the surface. Minimization of the surface energy might play a role in the formation of such islands. Comparing the morphology of the oxide films with the I - V characteristics reveals that even at a small thickness of the oxide film (~ 3 nm), the device per-

formance is governed by the oxide-polymer contact. The performance of devices with oxides is much better in terms of the power efficiency as compared to the ITO-only device.

In conclusion, we have demonstrated the use of transition metal oxides, V_2O_5 and MoO_3 , as an efficient buffer layer for polymer PV devices. The oxide layer plays an important role in preventing an unwanted chemical reaction between the ITO and the active layer. The V_{OC} of the devices was observed to be independent of the work function of the metal oxide used. Also, devices with an oxide buffer layer had a similar, or better, performance than the devices with a PEDOT:PSS buffer layer. The highest power conversion efficiency of 3.3% was achieved for the PV devices with MoO_3 as the buffer layer.

This work was supported in part by the Office of Naval Research (N00014-01-1-0136, program manager Dr. Paul Armistead), and Air Force Office of Scientific Research (F49620-03-1-0101, program manager Dr. Charles Lee).

- ¹C. J. Brabec, N. S. Sariciftci, and J. C. Hummelen, *Adv. Funct. Mater.* **11**, 15 (2001).
- ²S. E. Shaheen, C. J. Brabec, N. S. Sariciftci, F. Padinger, T. Fromherz, and J. C. Hummelen, *Appl. Phys. Lett.* **78**, 841 (2001).
- ³F. Padinger, R. S. Rittberger, and N. S. Sariciftci, *Adv. Funct. Mater.* **13**, 85 (2003).
- ⁴K. M. Coakley and M. D. McGehee, *Chem. Mater.* **16**, 4533 (2004).
- ⁵C. J. Brabec, *Sol. Energy Mater. Sol. Cells* **83**, 273 (2004).
- ⁶C. Walduf, P. Schilinsky, J. Hauch, and C. J. Brabec, *Thin Solid Films* **451-452**, 503 (2004).
- ⁷G. Li, V. Shrotriya, J. Huang, Y. Yao, T. Moriarty, K. Emery, and Y. Yang, *Nat. Mater.* **4**, 864 (2005).
- ⁸W. L. Ma, C. Y. Yang, X. Kong, K. Lee and A. J. Heeger, *Adv. Funct. Mater.* **15**, 1617 (2005).
- ⁹L. S. Roman, M. Berggren, and O. Inganäs, *Appl. Phys. Lett.* **75**, 3557 (1999).
- ¹⁰L. S. Roman, W. Mammo, L. A. A. Petersson, M. R. Andersson, and O. Inganäs, *Adv. Mater. (Weinheim, Ger.)* **10**, 774 (1998).
- ¹¹A. C. Arias, M. Granström, D. S. Thomas, K. Petritsch, and R. H. Friend, *Phys. Rev. B* **60**, 1854 (1999).
- ¹²F. L. Zhang, A. Gadisa, O. Inganäs, M. Svensson, and M. R. Andersson, *Appl. Phys. Lett.* **84**, 3906 (2004).
- ¹³M. P. de Jong, L. J. van Ijzendoorn, and M. J. A. de Voigt, *Appl. Phys. Lett.* **77**, 2255 (2000).
- ¹⁴K. W. Wong, H. L. Yip, Y. Luo, K. Y. Wong, W. M. Lau, K. H. Low, H. F. Chow, Z. Q. Gao, W. L. Yeung, and C. C. Chang, *Appl. Phys. Lett.* **80**, 2788 (2002).
- ¹⁵T. P. Nguyen and S. A. de Vos, *Surf. Sci.* **221**, 330 (2004).
- ¹⁶J. Kido, T. Matsumoto, T. Nakada, J. Endo, K. Mori, N. Kawamura, and A. Yoko, *SID 2003*, p. 964.
- ¹⁷G. L. Frey, K. J. Reynolds, and R. H. Friend, *Adv. Mater. (Weinheim, Ger.)* **14**, 265 (2002).
- ¹⁸K. J. Reynolds, J. A. Barker, N. C. Greenham, R. H. Friend, and G. L. Frey, *J. Appl. Phys.* **92**, 7556 (2002).
- ¹⁹V. D. Mihailetschi, L. J. A. Koster, and P. W. M. Blom, *Appl. Phys. Lett.* **85**, 970 (2004).
- ²⁰V. D. Mihailetschi, P. W. M. Blom, J. C. Hummelen, and M. T. Rispen, *J. Appl. Phys.* **94**, 6849 (2004).
- ²¹L. J. Brillson, *Surf. Sci. Rep.* **2**, 123 (1986).
- ²²J. M. Bharathan and Y. Yang, *J. Appl. Phys.* **84**, 3207 (1998).
- ²³C. J. Brabec, A. Cravino, D. Meissner, N. S. Sariciftci, T. Fromherz, M. T. Rispen, L. Sanchez, and J. C. Hummelen, *Adv. Funct. Mater.* **11**, 374 (2001).
- ²⁴C. J. Brabec, S. E. Shaheen, C. Winder, and N. S. Sariciftci, *Appl. Phys. Lett.* **80**, 1288 (2002).